

Integrating Kinetic Models, Gene Circuits, and Biofilm Dynamics for Enhanced Exopolysaccharide Production in Nitrifying Bacterial Consortia

Indhuja Sakthivel¹, Boobal Rangaswamy^{1*}, Bharathkumar Rajagopal², Lathika Shanmugam¹

¹*Department of Biotechnology, PSG College of Arts & Science, Coimbatore, Tamil Nadu 641014, India*

²*Amity Institute of Biotechnology, Amity University Uttar Pradesh, Noida 201313, India*

1 *Corresponding author. E-mail address: boobal@psgcas.ac.in (Boobal Rangaswamy)

ORCID: 0000-0002-8270-9755 (Boobal Rangaswamy)

2 **Abstract**

3 Bacterial consortia with extracellular polysaccharides (EPS) serves as key functional components in sustainable
4 wastewater treatment and pollutant removal. This study integrates kinetic modelling and synthetic biology to
5 optimize EPS production and nitrogen removal in a bacterial consortium enriched from domestic wastewater.
6 Employing Monod and Verhulst models, consortia growth was simulated under controlled nitrogen flux (10 ppm
7 NH_4Cl), achieving a maximum biomass concentration ($\text{OD}_{590} = 5.39$) and EPS yield of 2.63 g/mL by day 45. SEM
8 analysis revealed progressive biofilm maturation, transitioning from sparse aggregates to dense EPS-embedded
9 matrices. Nitrogen flux analysis demonstrated efficient substrate utilization, with 80% ammonia oxidized by
10 autotrophic populations (AOB/NOB). PCR amplification confirmed the presence of the *exoY* gene, central to EPS
11 biosynthesis, enabling the design of a BUFFER-gate logic circuit to regulate succinoglycan production. The
12 consortium's dual capacity for nitrification and denitrification, coupled with high EPS yields, underscores its
13 potential for enhancing wastewater treatment efficiency and biofilm engineering. These findings provide a
14 framework for leveraging microbial consortia in bioremediation and industrial biotechnology through targeted
15 genetic and kinetic optimisation.

16

17 **Keywords:** Bacterial-consortia, EPS, wastewater treatment, Monod model, Verhulst model, logic circuits

18

19 1. Introduction

20 Microbial consortia are dynamic assemblages of bacteria increasingly utilised for their pollutant-removal
21 capabilities, particularly in biological wastewater treatment systems, where EPS play a pivotal role. Microbial
22 consortia offer a cost-effective, eco-friendly alternative to conventional wastewater treatments, leveraging their
23 high biodegradation efficiency to reduce pollutants. The consortium helps to enhance the wastewater quality by
24 decreasing the odour and colour, thereby improving the value of treatment plants (Del Nery et al., 2016).
25 Compared to traditional methods such as chemical treatments and membrane filtration, bacterial biofilms reduce
26 sludge accumulation in large-scale wastewater treatment systems, enhancing operational sustainability (He et al.,
27 2023). The extracellular matrix of bacterial biofilms mostly consists of proteins, nucleic acids, and dead cells,
28 playing a key role in cell-cell communication (Heilmann & Götz, 2009). The formation of consortia is complex,
29 as it includes bacteria from different species growing on surfaces to produce EPS. Chen et al. (2021) identified
30 common bacteria found in biofilms such as *Pseudomonas aeruginosa*, *Staphylococcus epidermidis*, *Escherichia*
31 *coli*, *Klebsiella pneumoniae*, *Proteus mirabilis*, *Streptococcus viridans*, *Staphylococcus aureus*, and *Enterococcus*
32 *faecalis*. Proteins and polysaccharides are the main components of EPS (Zhao et al., 2019). EPS also comprises
33 uronic acids, humic acids, lipids, and inorganic elements (Guibaud et al., 2012). According to Freire-Nordi et al.,
34 (2005), research found that EPS with uronic acid and sulphates can immobilise positively charged metal ions,
35 which is beneficial for water purification. Various factors including the source of sludge, the type of wastewater,
36 and operational conditions influence the composition and concentrations of EPS in sludge aggregates (Yuan et
37 al., 2017). Microbial biofilm might play role in affecting their structure, surface charge, flocculation, settling,
38 dewatering, and adsorption properties in sewage treatment facilities (Sheng et al., 2010). Additionally, EPS has
39 shown potential in environmental remediation by facilitating the removal of pollutants and heavy metals from
40 contaminated areas. The consortium-associated EPS functions in cleaning up the environment (Bhattacharya et
41 al., 2019). Moreover, EPS has exhibited potential in biotechnological research, particularly in the production of
42 enzymes and antibiotics (Andrew & Jayaraman, 2020), and is commonly utilised in the food (Suryawanshi et al.,
43 2022), cosmetics, and pharmaceutical (Wao et al., 2023) sectors due to its favourable physical, rheological, and
44 safety properties (Xiong et al., 2022). Quorum sensing (QS) regulation has been identified as the most extensively
45 studied regulatory mechanism responsible for controlling the production of EPS, biofilm formation, and
46 differentiation (Yadav et al., 2023; Zhou et al., 2025).

47 Nitrifying bacteria include ammonia-oxidizing bacteria (AOB) and nitrite-oxidizing bacteria (NOB),
48 which are found in both autotrophs and heterotrophs. Moreover, autotrophic and heterotrophic consortia bacteria

49 remove heavy metals and nutrients (phosphate and nitrate) from the wastewater and stabilise the downstream
50 treatment process. Autotrophic bacteria gain energy by oxidizing ammonia to nitrates and nitrites or utilizing
51 organic substances as a nitrogen source (Vajda et al., 2011; Xia et al., 2019). Nitrifying consortia enhance EPS
52 production due to their role in microbial granulation and environmental adaptability. These factors contribute to
53 the stability and efficiency of wastewater treatment processes, making nitrifying consortia particularly effective
54 in EPS enhancement (Li et al., 2020; Song et al., 2020).

55 In bioremediation, the functions of AOB and NOB have been examined using a combination of
56 physiological and molecular in situ techniques (Cai et al., 2018). As various genes related to the synthesis of EPS
57 (exo, epsE, eps9F, epsH, and epsF) are involved in forming the consortia structure, they play a significant role in
58 the advancement of consortia (Janczarek, 2011). In a recent study Wang et al., (2023) reported that the EPS from
59 *Streptococcus thermophilus* has significant applications in the dairy industry and probiotics. Gaining insights into
60 the impact of nitrogen sources on EPS production can optimise fermentation processes, enhance the texture and
61 health benefits of fermented dairy products, and improve the overall functionality of probiotic strains (Korcz &
62 Varga, 2021).

63 Various mathematical models have been proposed to describe the changing aspects of the metabolism of
64 compounds exposed to cultures of microbial populations of the natural environment (Smith et al., 1997).
65 According to Hwi Jeong & Min Lee, (2013), most growth models rely on Monod kinetics and require the
66 measurement of several parameters. The Monod model is widely used to demonstrate growth-linked substrate
67 utilization. Additionally, Liu, (2006) highlighted the Monod equation as a highly effective model for
68 demonstrating the relationship between specific growth rate and required substrate concentration. (Ruiz et al.,
69 2013) simulated bacterial biomass growth rate using the Verhulst kinetic model. Dmitry Dvoretzky et al., (2015)
70 used Verhulst logical equation for modelling biomass cultivation process. This research aims to enhance the
71 productivity of wastewater treatment plants by integrating the Monod and Verhulst models for consortium
72 bacterial growth. The highest biomass concentration of EPS-producing species significantly increases the
73 consortium growth that occurred at the biofilm-liquid interface (Kreft & Wimpenny, 2001). The Monod/Verhulst
74 model is adept at managing the complex non-linear dynamics typical of microbial EPS production processes,
75 which traditional models with single-factor experiments may not accurately predict (Marques et al., 2017; Plattes
76 & Lahore, 2023).

77 The gene circuit model using the logic gates represents high advancement in the field of synthetic biology
78 (Lezia et al., 2022). In this study we also focused on developing a gene circuit which helps us to understand how

79 to regulate the production of EPS by the expression of the required gene, which enables bacteria to adapt to
80 environmental signals and enhance EPS production by maximizing nitrogen source utilization. Overall,
81 optimizing substrate flux kinetics and the development of gene circuits can help us to enhance EPS production
82 efficiency in microbial consortia. Hence, this study aims to construct a logic gene circuit for the EPS pathway in
83 consortia-forming bacteria and to assess their growth kinetics, structural properties, and wastewater treatment
84 potential.

85

86 2. Materials and methods

87 2.1 Sample collection and Synthetic medium preparation

88 The sludge sample was collected from the domestic wastewater treatment plant in Coimbatore. The
89 sample was transferred to the lab and stored at 4°C. Modified synthetic media was prepared following (0.3g KCl,
90 0.5g KH₂PO₄, NaCl 2.5, 0.02g NH₄Cl, 0.04g K₂HPO₄, 1.6g of Na₂CO₃, CaCO₃ 0.03, 0.5g of CaCl₂, and 5g starch
91 (Youssef et al., 2016). The sample inoculated culture flasks were placed in the shaker incubator at 37°C with the
92 revolution set at 150 rpm, an optimal temperature and pH were maintained throughout the study period.

93 2.2 Consortia development

94 The culture was enriched with NH₄Cl of 10 ppm for every two days. This addition will provide the
95 microorganisms with a nitrogen source that influences the formation of nitrogen utilizing population. The growth
96 of the bacterial consortia is regularly measured and growth kinetics was determined (Hamzah et al., 2013). The
97 increase in the growth ratio correlated with the increase in the biomass of the culture.

98 2.3 Mathematical modeling and kinetic expression of consortia growth

99 This study aimed to predict the consortia development by employing the mathematical model (Sadiq et
100 al., 2018) and focused specifically on nitrogen utilization as a substrate. The Monod model expressed growth
101 kinetics utilizing the relationship between growth and substrate concentration.

$$102 \quad \mu = \mu_{max} \left[\frac{S_i}{k_i + S_i} \right] \quad (1)$$

103 Where the specific growth rate is represented by μ , the substrate concentration is denoted as S_i , μ_{max} stands for
104 the maximum specific growth rate and the saturation constant is k_i . Since focused solely on a single substrate
105 type, the specific growth rate, μ can be expressed as

$$106 \quad \mu = \mu_{max} \left[\frac{S_N}{K_N + S_N} \right] \quad (2)$$

107 where S_N represents the concentration of nitrogen in the medium and k_N is the half-saturation constant for
108 nitrogen. The specific growth rate utilised in this study is an expansion of the Monod model.

109 The Verhulst model is expressed as described in (Abdel-Raouf et al., 2012).

$$110 \quad X(t) = \frac{X_m X_0 e^{\mu t}}{X_m - X_0 + X_0 e^{\mu t}} \quad (3)$$

111 where x represents the biomass concentration of biofilm, x_m represents the maximum cell concentration that the
112 system can reach in batch, X_0 is initial concentration of microorganism, t represents time and μ is the specific
113 growth rate of the biofilm. The specific growth rate in the extended Monod model (2) is substituted into the
114 Verhulst model (3) to estimate the consortia growth.

115 **2.4 Mathematical modeling and kinetic expression for nutrient uptake by consortia**

116 The equation representing the Verhulst model was used to precisely explain the nutrient absorption by
117 the consortia (Álvarez-Díaz et al., 2017).

$$118 \quad \left(\frac{X_0}{Y} + S_0\right) (S_0 - S_{na}) - S_{na} \left(\frac{X_0}{Y} + S_0\right) \quad (4)$$

$$119 \quad S = \frac{\left(\frac{X_0}{Y} + S_0\right) (S_0 - S_{na}) - S_{na} \left(\frac{X_0}{Y} + S_0\right)}{(S_0 - S_{na}) - \left(S_0 - \left(\frac{X_0}{Y} + S_0\right)\right) e^{pt}}$$

120 where S is the total nutrient concentration, S_0 represents the initial amount of substrate concentration in the culture
121 medium, S_{na} is the unassimilated substrate concentration and p denotes the specific consortia growth rate and Y
122 is the consortia yield coefficient for the ratio of biomass produced per mass of substrate incorporated as organic
123 or structural which can be calculated using the equation as stated below

$$124 \quad Y = \left[\frac{X_m - X_0}{S_b - S_{na}} \right] \quad (5)$$

125 By some transformations to (4) as outlined in the study by Álvarez-Díaz et al., (2017), the equation can be
126 modified to resemble equation (3)

127 Hence, conclude that p indicates the specific growth rate of consortia, μ and t have the same relation to estimate
128 consortia growth and nutrient uptake by using the Verhulst model. Therefore, the specific growth rate, μ of the
129 extended Monod model in (2) will be used in place of p for nutrient absorption by the consortium.

$$130 \quad X(t) = \frac{X_m X_0 e^{\mu t}}{X_m - X_0 + X_0 e^{\mu t}} \quad (6)$$

131 **2.5 EPS determination and quantification**

132 The consortia were centrifuged at 12,000 rpm for 15 minutes (sigma 2-16KL, Germany). The supernatant
133 with 95% cold ethanol was vigorously stirred and then kept for 24 h at 4°C to ensure complete EPS precipitation.
134 Subsequently, the precipitates were collected by centrifugation at 12,000 rpm for 20 minutes. The pellet was dried
135 overnight at 60°C (Padmanaban et al., 2015). The recovered EPS was figured out gravimetrically by grams per

136 mL of culture medium and then made to dry. The dried EPS was weighed for up to 45 days during the culture
137 process.

138 **2.6 Characterization of morphology**

139 The consortium culture was incubated and the pellet was collected using an ultrafiltration after seven
140 days of growth. The pellet was dried and then analysed using SEM to evaluate the growth of consortia and the
141 increase in EPS production within the consortia. The same process was repeated on the 45th day of growth to
142 evaluate any changes during the incubation period (Rangaswamy et al., 2020).

143 **2.7 Physiochemical properties of ammonia, nitrite, nitrate, and nitrogen flux**

144 To determine the effectiveness of the nitrification process in the consortia sample that was fed with
145 NH₄Cl, the levels of ammonia, nitrate, and nitrite values in the samples were estimated and noted by the phenate
146 method (Joseph et al., 2021). The values were measured before feeding, during feeding, and after feeding of
147 NH₄Cl.

148 **2.7.1 Estimation of ammonia**

149 1 mL of sample was taken with 0.4 mL of sodium nitroprusside solution, 1 mL of oxidizing solution (100
150 mL of alkaline reagent was added to 25 mL of sodium hypochlorite and was mixed) was added, and made up to
151 10 mL of double-distilled water. The mixture was then incubated for 1h at room temperature. The reading was
152 noted at an absorbance of 640 nm using a UV-vis spectrometer (Solórzano, 1969).

153 **2.7.2 Estimation of nitrite**

154 The 10 mL of a sample was added with 0.2 mL of sulphanilamide solution and 0.2 mL of NED. The
155 reading was taken after 8 minutes at the absorbance of 543 nm.

156 **2.7.3 Estimation of nitrate**

157 A mixture was prepared by adding 10mL of the sample, 0.4 mL of buffer reagent (phenol solution and
158 NaOH 1:1 ratio), 0.2mL of hydrazine sulphate, CuSO₄ in a 1:1 ratio and then incubated in the dark for 18-24 hours
159 and again added 0.4mL of acetone, 0.2 mL sulphanilamide, and 0.2 mL NED. The reading was measured after 8
160 min at the absorbance of 543 nm.

161 **2.8 Determination of inorganic nitrogen flux**

162 The inorganic nitrogen fluxes in the consortia sample were calculated using the following equation (Yan
163 et al., 2024).

164
$$F = \frac{\Delta C.V}{A.\Delta t}$$

165 where F ($\text{mg m}^{-2}\text{d}^{-1}$) represents inorganic nitrogen fluxes; V (m^3) is the volume of the flask; A (m^2) is the
166 bottom area of the flask; Δt (d) denotes the incubation duration; and $\Delta C(\frac{\text{mg}}{\text{l}})$ stands the change in the
167 concentrations of ammonia, nitrite, and nitrate before and after incubation.

168 **2.9 DNA extraction**

169 Genomic DNA was isolated from the sediment using the protocol described by (Araya et al., 2003) with
170 slight modifications. The extracted DNA was added with 10 mL of CTAB buffer and tube was vortexed and
171 placed in a shaking incubator for 10 minutes at 60°C. Subsequently, it was centrifuged at 4000rpm for 15 minutes
172 to separate layers. The supernatant was added with cool Isopropanol and 5M NaCl. Stored at -20°C for overnight.
173 After centrifugation at 4000 rpm for 15 minutes, the entire solution was removed from the pellet. 2 mL of 70%
174 ethanol was added to the tube and centrifuged at 4000 rpm for 2 minutes. The rest of the ethanol was discarded
175 and dried for 30 minutes. 10 mM 20 μl of Tris HCl was added and the collected samples were subsequently
176 stored at -20°C.

177 **2.10 PCR and confirmation of amplicons**

178 PCR was used to screen the *exoY* gene to detect the presence of EPS in the genomic DNA sample from
179 the consortium bacteria with the forward and reverse primers sequence, 5'-ATGCGTATCGACGGTCATC- 3'
180 and 5'CCGAGGGGGGTGTATCTGACCC-3'. The PCR reaction was carried out at a total volume of 10 μL as
181 follows: 5 μL of Amp GT PCR master mix (Takara Bio Inc), 0.4 μL of both forward and reverse primers each,
182 3.8 μL of DNA template, and made up to 10 μL final volume with molecular grade water. The PCR conditions were
183 carried out as an initial denaturation step (at 95°C for 5 min), followed by 37 cycles of repetitions of denaturation
184 (at 95°C for 10 sec), annealing at 58°C, extension at 72°C for 1.30 sec with the final extension at 72°C for 10
185 minutes (Araya et al., 2003). Aliquots of PCR products were analysed by electrophoresis in 1 (w/v) molecular
186 grade agarose (Sigma-Aldrich, USA) gels containing ethidium bromide (0.5 mg mL⁻¹).

187 **2.11 Orthology of functional genes and Logic circuit of the pathway**

188 The gene circuit was constructed to map regulatory interactions governing EPS biosynthesis in nitrifying
189 consortia, using Boolean logic principles adapted from Boscaino et al., (2019). The EPS functional genes for all
190 consortia-forming bacterial groups in the Kyoto Encyclopedia of Genes and Genomes (KEGG) database were
191 extracted from the datasets. KEGG programming interface information regarding the gene orthology of the
192 bacterial organisms was obtained. The orthology content of each organism was converted into a binary logical
193 content vector denoted by "1" (indicating the presence of the ortholog) and "0" (indicating its absence) among all
194 orthologs found in the KEGG database. Modeling circuits of biological pathways focuses on the active events that

195 lead to activation. Entries are compared in G_{Erel} based on the selection of genes in the initial two
196 consecutive reactions.

197 **2.12 Statistical analysis**

198 Statistical analysis was performed to assess the significance of the results. A one-way ANOVA was utilized to
199 estimate the statistical parameters.

200 **3. Results**

201 **3.1 Consortia development**

202 The extended Monod and Verhulst models were used to estimate consortia growth on the 45th day in
203 domestic wastewater (**Table 1**). **Fig. 1** shows consortia growth in wastewater treatment plants, and the maximum
204 cell concentration on the 45th day OD value was 5.39. The sustained increase in OD values throughout the
205 incubation period signifies strong consortia development and maturation, highlighting the importance of long-
206 term culture techniques in studying consortium development. The consortia development values were statistically
207 significant ($p < 0.0005$).

208 **3.2 Characterization of Consortia**

209 Therefore, the SEM examination of consortia development revealed distinct differences between the
210 initial seven days (**Fig. 2a**) and the 45th day of culture growth. During the early stages, the consortia exhibited a
211 sparse and irregular structure with less complexity in the cell structure. In contrast to the 45th day, the consortium
212 growth has significantly increased in complexity, displaying a dense network of clustered cells embedded with a
213 well-developed extracellular matrix and the morphological characteristics of consortia were rod-shaped as
214 expressed in **Fig. 2b and 2c**. SEM analysis of the consortium culture on the initial 10th day showed minimal EPS
215 presence despite the denser EPS matrix interaction among microorganisms (**Fig. 2d**). By the 45th day, cells
216 exhibited a dense network and superior complexity due to increased EPS formation and well-developed EPS
217 structures (**Fig. 2e and 2f**).

218 **3.3 EPS formation**

219 The growth of EPS in the culture medium was gradually increased, enhancing the consortia growth and
220 the maximum EPS production on the 45th day was 2.63 g/mL. These results, as given in **Fig. 3**, statistically
221 significantly prove consortia growth, which determines the high production of EPS ($p < 0.05$).

222 **3.4 Substrate utilization and nitrogen flux resembling autotrophic population**

223 The consortia culture was fed with NH_4Cl at an initial concentration of 10 ppm. The amount of ammonia,
224 nitrite, and nitrate was estimated by the phenate method. Therefore, 8 ppm (*avg.*) of ammonia has been utilised
225 by the AOB population for ammonia oxidation and 2 ppm (*avg.*) becomes an unassimilated substrate. Further, in
226 the next process, 5 ppm of ammonia was transferred for the conversion of nitrite formation, and 4.2 ppm (*avg.*)
227 was utilised by the NOB population for nitrite oxidation leaving 0.8 ppm (*avg.*) of unutilised substrate. NOB
228 further transforms 4ppm of nitrite which was effectively transferred to form nitrate. From the estimation of nitrate
229 by phenate method, 2.4 ppm (*avg.*) was utilised by the bacteria and the remaining 1.6 ppm enters into the
230 denitrification process for further metabolism. Therefore, the initial and final substrate concentrations of the
231 nitrogen source were 10 ppm and 2 ppm. This shows that the nitrogen was reduced drastically, proving that the
232 consortia in the wastewater removed the nitrogen which proves treating wastewater efficiently. This analysis
233 highlights how autotrophic bacteria in consortia culture utilise substrates, focusing on the contributions of AOB
234 and NOB populations (**Fig. 5**). The nitrogen substrate was consumed by the AOB and NOB populations via the
235 processes of nitrification to nitration. In contrast to this, the changes in the nitrogen source concentration from the
236 nitrogen flux (**Fig. 4**) in the consortium culture were also estimated for 45 days which typically involves measuring
237 the changes in the concentrations of nitrogen compounds (ammonia, nitrite, and nitrate) in the culture after feeding
238 the culture with NH_4Cl at the same concentration of 10 ppm (**Fig. 5**). The statistical analysis evidence showed
239 moderately significant ($p>0.1$).

240 **3.5 PCR and confirmation of amplicons**

241 The *exoY* gene primer was used to identify the presence of EPS in the consortia sample and produced a
242 DNA fragment between 200-250 bp when annealed at 55°C. Agarose gel image for the obtained PCR product (In
243 well 1, T_a was 51°C; in well 2, T_a was 52°C; in well 3, T_a was 53°C and in well 4 is NTC followed by a 50bp
244 molecular marker in well 5).

245 **3.6 Construction of logic circuits from the amplified PCR product**

246 PCR amplification and orthology data from the KEGG database identified *exoY* as the sole amplifiable
247 gene linked to EPS synthesis in the consortium, prompting its selection as the circuit's central node. Binary logic
248 gates were defined as follows: A BUFFER gate represented direct, unconditional activation, where *exoY* presence
249 (input = 1) leads to the activation of *ExoL* which in turn triggered EPS production (output = 1). AND gates were
250 reserved for hypothetical auxiliary interactions, but no co-activators were amplified, limiting the circuit to a
251 simplified BUFFER architecture. OR gates were omitted due to the absence of redundant EPS genes. The logic

252 circuit, structured around a BUFFER gate (**Fig. 6**), mapped *exoY* activation directly to *exoL* gene which in turn
253 linked to succinoglycan (EPS) biosynthesis (Reuber & Walker, 1993).

254 4. Discussion

255 4.1 EPS Production Dynamics and Biofilm Structural Maturation

256 The synthesis of EPS by bacterial consortia is intrinsically linked to biofilm maturation, as evidenced by
257 the progressive increase in EPS yield (2.63 g/mL on day 45) and SEM-derived morphological changes. The sparse,
258 irregular biofilm structure observed during the initial seven days transitioned to a dense, interconnected matrix by
259 day 45 (**Fig. 2a–f**), corroborating the role of EPS in stabilising microbial aggregates. This aligns with studies
260 emphasising EPS as a structural scaffold that facilitates cell adhesion and nutrient retention within biofilms
261 (Bhawal et al., 2022; Zhao et al., 2019). The SEM-derived biofilm architecture corroborates Wang et al., (2023)
262 who linked structural complexity to the choice of substrate. However, further studies are recommended. The rod-
263 shaped morphology of consortia members, consistent with *Rhizobium* *sps.*, (Kaur et al., 2011), and *Pseudomonas*
264 *sps.*, (Gangalla et al., 2021), along with the findings of *exoY* gene, suggests that particular rod shaped bacterial
265 taxa dominate the consortium, potentially contributing to the observed EPS overproduction (Chen et al., 2021;
266 Sellami et al., 2015). The temporal correlation between biofilm complexity and EPS accumulation underscores
267 the necessity of prolonged incubation (45 days). However, achieving optimal EPS yields in a short period can be
268 further analyzed with gene expression studies, a critical factor for industrial applications requiring high
269 biopolymer output in a relatively short amount of time.

270 The gravimetric quantification of EPS revealed a gradual increase, peaking at 2.63 g/mL by day 45 (**Fig.**
271 **3**). This trend mirrors microbial growth phases, where EPS production is elevated during exponential growth due
272 to active nutrient assimilation and declines during stationary phases due to resource depletion. The sustained EPS
273 synthesis in this study, however, contrasts with earlier reports of peak EPS yields of 0.042g/ml in 96 hours
274 (Sellami et al., 2015), highlighting the advantage of consortium-based systems over monocultures in prolonging
275 productive phases. The observed EPS yield surpasses values reported for monocultures like *Pseudomonas*
276 *aeruginosa*, *Micrococcus* *sps.* (Yin et al., 2022) and *L. plantarum* (Zhang et al., 2023), underscoring the advantage
277 of consortia in leveraging metabolic diversity. The integration of ammonium chloride as a nitrogen source likely
278 enhanced autotrophic nitrifier activity, further driving EPS biosynthesis through metabolic synergy between
279 ammonia-oxidizing bacteria (AOB) and nitrite-oxidizing bacteria (NOB). Moreover, discrepancies in optimal pH

280 (Jyoti et al., 2024) and incubation duration (Sellami et al., 2015) highlight context-dependent variability in EPS
281 production, necessitating strain-specific optimisation.

282 **4.2 Kinetic Modelling of Consortium Growth and Substrate Utilisation**

283 The Monod and Verhulst models provided robust frameworks for analysing consortium growth kinetics
284 and nitrogen substrate utilisation. The Monod-derived maximum specific growth rate ($\mu_{\max} = 5.39$) and half-
285 saturation constant ($k_n = 2.69$) (**Table 1**) reflect efficient nitrogen assimilation, particularly under high substrate
286 availability ($S_n = 10$ ppm). The Verhulst model further shows that biomass accumulation, predicting a maximum
287 cell concentration ($X_m = 1.63$) that aligns with the observed OD₅₉₀ of 5.39 (**Fig. 1**). The nitrogen flux analysis
288 revealed that AOB oxidised 80% of the initial ammonium (8 ppm), while 42% of nitrite (4.2 ppm) was further
289 metabolised by NOB. The residual nitrate (1.6 ppm) entering denitrification pathways underscores the
290 consortium's dual role in nitrification and partial denitrification, a trait advantageous for wastewater treatment.

291 **4.3 Gene Circuit Engineering and *exoY* Amplification in EPS Biosynthesis**

292 The exclusive amplification of *exoY* gene highlights its dominant role in EPS biosynthesis within the
293 consortium. KEGG orthology traces *exoY* to Rhizobiaceae, suggesting Rhizobium-related species, which is
294 known for its symbiotic nitrogen fixation and succinoglycan production which may dominate the consortium
295 (Jones, 2012; Ratib et al., 2018). While Rhizobium is not classically autotrophic, its presence could synergise with
296 undetected ammonia-oxidizing bacteria (AOB), as Rhizobium-derived EPS may stabilise biofilms, enhancing
297 retention of autotrophic nitrifiers. The observed nitrification efficiency likely arises from such metabolic
298 partnerships, where Rhizobium's heterotrophic activity complements autotrophic ammonia oxidation by AOB.
299 The BUFFER gate's simplicity reflects the consortium's reliance on *exoY* driven EPS synthesis. Moreover, the
300 consortium's higher EPS yield (2.63 g/mL) suggests that using EPS producing bacterial consortium in water
301 treatment plants, particularly by over expressing *exoY* gene is promising when compared to single strains ($9.2 \pm$
302 0.66 g/L in *Rhizobium leguminosarum*) used in previous studies (Sellami et al., 2018). Future work could integrate
303 inducible promoters to further enhance EPS titres.

304 **4.4 Implications for Wastewater Treatment and Biotechnological Applications**

305 The consortium's ability to reduce ammonium from 10 ppm to 2 ppm over 45 days demonstrates its
306 efficacy in nitrogen removal, a critical metric for wastewater treatment. However, enhancing *exoY* gene
307 expression might reduce this time frame further. The sequential oxidation of ammonia to nitrate, coupled with
308 partial denitrification, could be a sustainable alternative to traditional methods. The EPS matrix's metal-binding

309 capacity, attributed to uronic acids and sulphates (Freire-Nordi et al., 2005), positions the consortium as a
310 candidate for bioremediation of heavy metal-laden effluents. This opens the door for further research in the field
311 of bioremediation.

312 **5. Conclusion**

313 This study demonstrates the synergistic potential of microbial consortia in wastewater treatment, driven
314 by EPS-mediated biofilm development and nitrogen metabolism. By coupling Monod and Verhulst kinetic
315 models, consortia growth and substrate utilisation were accurately predicted, achieving maximal EPS production
316 (2.63 g/mL) and 80% nitrogen removal over 45 days. SEM imaging validated biofilm structural maturation,
317 correlating EPS accumulation with microbial aggregation. The identification of the *exoY* gene and subsequent
318 logic circuit design highlighted its pivotal role in regulating EPS biosynthesis, offering a genetic toolkit for
319 enhancing biopolymer yields. Future work should explore *exoY* overexpression under inducible promoters to
320 accelerate EPS production and investigate field-scale applications for heavy metal bioremediation. This
321 integrative approach is bridging kinetic modeling, genetic circuitry, and microbial ecology and advances the
322 rational design of consortia for environmental and industrial applications.

323

324 **Acknowledgment**

325 The authors are grateful to the Department of Science and Technology (DST), Government of India, New Delhi,
326 India for the financial support of the research facility at PSG College of Arts & Science College, Coimbatore,
327 India as part of Fund for the Improvement of S & T Infrastructure (DST – FIST).

328 **Conflict of interest**

329 The authors declare that they have no conflict of interest.

330 **Informed consent statement**

331 Not applicable.

332 **Consent to publish**

333 All authors approved the manuscript and gave their consent for submission and publication.

334 **Data availability statement**

335 There is no research related data stored in publicly available repositories, and the data will be made available on
336 request.

337 **Declaration of Interest Statement**

338 The authors declare that they have no known competing financial interests or personal relationships that could
339 have appeared to influence the work reported in this paper.

340 **Author contribution**

341 **Indhuja Sakthivel:** Methodology, Validation, Formal analysis, Writing - Original Draft. **Boobal Rangaswamy:**
342 Conceptualization, Methodology, Validation, Formal analysis, Visualization, Data curation, Writing – original
343 draft, Writing –review & editing, Supervision, Investigation. **Bharathkumar Rajagopal:** Writing - Original
344 Draft, Writing - Review & Editing. **Lathika Shanmugam:** Data Curation, Visualization, Writing - Original Draft,
345 Writing - Review & Editing.

346 **Declaration of competing interest**

347 The authors declare that they have no known competing financial interests or personal relationships that could
348 have appeared to influence the work reported in this paper.

349 **Funding**

350 This research did not receive any specific grant from funding agencies in the public, commercial, or not-for-profit
351 sectors.

352

353 **References**

- 354 1. Abdel-Raouf, N., Al-Homaidan, A. A., & Ibraheem, I. B. M. (2012). Microalgae and wastewater
355 treatment. *Saudi Journal of Biological Sciences*, 19(3), 257–275.
356 <https://doi.org/10.1016/j.sjbs.2012.04.005>
- 357 2. Álvarez-Díaz, P. D., Ruiz, J., Arbib, Z., Barragán, J., Garrido-Pérez, M. C., & Perales, J. A. (2017).
358 Freshwater microalgae selection for simultaneous wastewater nutrient removal and lipid production.
359 *Algal Research*, 24, 477–485. <https://doi.org/10.1016/j.algal.2017.02.006>
- 360 3. Andrew, M., & Jayaraman, G. (2020). Structural features of microbial exopolysaccharides in relation to
361 their antioxidant activity. *Carbohydrate Research*, 487, 107881.
362 <https://doi.org/10.1016/j.carres.2019.107881>
- 363 4. Araya, R., Tani, K., Takagi, T., Yamaguchi, N., & Nasu, M. (2003). Bacterial activity and community
364 composition in stream water and biofilm from an urban river determined by fluorescent in situ
365 hybridization and DGGE analysis. *FEMS Microbiology Ecology*, 43(1), 111–119.
366 <https://doi.org/10.1111/j.1574-6941.2003.tb01050.x>
- 367 5. Bhattacharya, M., Guchhait, S., Biswas, D., & Singh, R. (2019). Evaluation of a microbial consortium
368 for crude oil spill bioremediation and its potential uses in enhanced oil recovery. *Biocatalysis and*
369 *Agricultural Biotechnology*, 18. Scopus. <https://doi.org/10.1016/j.bcab.2019.101034>
- 370 6. Bhawal, S., Kumari, A., Kapila, S., & Kapila, R. (2022). Biofunctional Attributes of Surface Layer
371 Protein and Cell-Bound Exopolysaccharide from Probiotic *Limosilactobacillus fermentum* (MTCC
372 5898). *Probiotics and Antimicrobial Proteins*, 14(2), 360–371. [https://doi.org/10.1007/s12602-021-](https://doi.org/10.1007/s12602-021-09891-4)
373 [09891-4](https://doi.org/10.1007/s12602-021-09891-4)
- 374 7. Boscaino, V., Fiannaca, A., La Paglia, L., La Rosa, M., Rizzo, R., & Urso, A. (2019). MiRNA
375 therapeutics based on logic circuits of biological pathways. *BMC Bioinformatics*, 20(S9), 344.
376 <https://doi.org/10.1186/s12859-019-2881-7>
- 377 8. Cai, M., Ng, S.-K., Lim, C. K., Lu, H., Jia, Y., & Lee, P. K. H. (2018). Physiological and Metagenomic
378 Characterizations of the Synergistic Relationships between Ammonia- and Nitrite-Oxidizing Bacteria in
379 Freshwater Nitrification. *Frontiers in Microbiology*, 9, 280. <https://doi.org/10.3389/fmicb.2018.00280>
- 380 9. Chen, C., Ali, A., Su, J., Wang, Y., Huang, T., & Gao, J. (2021). *Pseudomonas stutzeri* GF2 augmented
381 the denitrification of low carbon to nitrogen ratio: Possibility for sewage wastewater treatment.
382 *Bioresource Technology*, 333. Scopus. <https://doi.org/10.1016/j.biortech.2021.125169>

- 383 10. Del Nery, V., Damianovic, M. H. Z., Moura, R. B., Pozzi, E., Pires, E. C., & Foresti, E. (2016). Poultry
384 slaughterhouse wastewater treatment plant for high quality effluent. *Water Science and Technology*,
385 73(2), 309–316. <https://doi.org/10.2166/wst.2015.494>
- 386 11. Dmitry Dvoretzky, Stanislav Dvoretzky, Evgenya Peshkova, & Mikhail Temnov. (2015). Optimization
387 of the process of cultivation of microalgae *Chlorella vulgaris* biomass with high lipid content for biofuel
388 production. *Chemical Engineering Transactions*, 43, 361–366. <https://doi.org/10.3303/CET1543061>
- 389 12. Freire-Nordi, C. S., Vieira, A. A. H., & Nascimento, O. R. (2005). The metal binding capacity of
390 *Anabaena spiroides* extracellular polysaccharide: An EPR study. *Process Biochemistry*, 40(6), 2215–
391 2224. <https://doi.org/10.1016/j.procbio.2004.09.003>
- 392 13. Gangalla, R., Sampath, G., Beduru, S., Sarika, K., Kaveriyappan Govindarajan, R., Ameen, F., Alwakeel,
393 S., & Thampu, R. K. (2021). Optimization and characterization of exopolysaccharide produced by
394 *Bacillus aerophilus* rkl and its in vitro antioxidant activities. *Journal of King Saud University - Science*,
395 33(5), 101470. <https://doi.org/10.1016/j.jksus.2021.101470>
- 396 14. Guibaud, G., Bhatia, D., d'Abzac, P., Bourven, I., Bordas, F., Van Hullebusch, E. D., & Lens, P. N. L.
397 (2012). Cd(II) and Pb(II) sorption by extracellular polymeric substances (EPS) extracted from anaerobic
398 granular biofilms: Evidence of a pH sorption-edge. *Journal of the Taiwan Institute of Chemical
399 Engineers*, 43(3), 444–449. <https://doi.org/10.1016/j.jtice.2011.12.007>
- 400 15. Hamzah, A., Phan, C.-W., Abu Bakar, N. F., & Wong, K.-K. (2013). Biodegradation of Crude Oil by
401 Constructed Bacterial Consortia and the Constituent Single Bacteria Isolated From Malaysia.
402 *Bioremediation Journal*, 17(1), 1–10. <https://doi.org/10.1080/10889868.2012.731447>
- 403 16. He, Y., Liu, Y., Li, X., Zhu, T., & Liu, Y. (2023). Unveiling the roles of biofilm in reducing N₂O
404 emission in a nitrifying integrated fixed-film activated sludge (IFAS) system. *Water Research*, 243.
405 Scopus. <https://doi.org/10.1016/j.watres.2023.120326>
- 406 17. Heilmann, C., & Götz, F. (2009). Cell–Cell Communication and Biofilm Formation in Gram-Positive
407 Bacteria. In *Bacterial Signaling* (pp. 7–22). John Wiley & Sons, Ltd.
408 <https://doi.org/10.1002/9783527629237.ch1>
- 409 18. Janczarek, M. (2011). Environmental signals and regulatory pathways that influence exopolysaccharide
410 production in rhizobia. *International Journal of Molecular Sciences*, 12(11), 7898–7933. Scopus.
411 <https://doi.org/10.3390/ijms12117898>

- 412 19. Jones, K. M. (2012). Increased production of the exopolysaccharide succinoglycan enhances
413 Sinorhizobium meliloti 1021 symbiosis with the host plant Medicago truncatula. *Journal of Bacteriology*,
414 *194*(16), 4322–4331. Scopus. <https://doi.org/10.1128/JB.00751-12>
- 415 20. Joseph, V., Chellappan, G., Aparajitha, S., Ramya, R. N., Vrinda, S., Rejish Kumar, V. J., & Bright
416 Singh, I. S. (2021). Molecular characterization of bacteria and archaea in a bioaugmented zero-water
417 exchange shrimp pond. *SN Applied Sciences*, *3*(4), 458. <https://doi.org/10.1007/s42452-021-04392-z>
- 418 21. Jyoti, K., Soni, K., & Chandra, R. (2024). Optimization of the production of Exopolysaccharide (EPS)
419 from biofilm-forming bacterial consortium using different parameters. *The Microbe*, *4*, 100117.
420 <https://doi.org/10.1016/j.microb.2024.100117>
- 421 22. Kaur, J., Verma, M., & Lal, R. (2011). Rhizobium rosettiformans sp. Nov., isolated from a
422 hexachlorocyclohexane dump site, and reclassification of Blastobacter aggregatus hirsch and müller
423 1986 as Rhizobium aggregatum comb. Nov. *International Journal of Systematic and Evolutionary*
424 *Microbiology*, *61*(5), 1218–1225. Scopus. <https://doi.org/10.1099/ijs.0.017491-0>
- 425 23. Korcz, E., & Varga, L. (2021). Exopolysaccharides from lactic acid bacteria: Techno-functional
426 application in the food industry. *Trends in Food Science & Technology*, *110*, 375–384.
427 <https://doi.org/10.1016/j.tifs.2021.02.014>
- 428 24. Kreft, J.-U., & Wimpenny, J. W. (2001). Effect of EPS on biofilm structure and function as revealed by
429 an individual-based model of biofilm growth. *Water Science and Technology*, *43*(6), 135–135.
430 <https://doi.org/10.2166/wst.2001.0358>
- 431 25. Lezia, A., Miano, A., & Hasty, J. (2022). Synthetic Gene Circuits: Design, Implement, and Apply.
432 *Proceedings of the IEEE*, *110*(5), 613–630. Scopus. <https://doi.org/10.1109/JPROC.2021.3134169>
- 433 26. Li, X., Du, R., Peng, Y., Zhang, Q., & Wang, J. (2020). Characteristics of sludge granulation and EPS
434 production in development of stable partial nitrification. *Bioresource Technology*, *303*, 122937.
435 <https://doi.org/10.1016/j.biortech.2020.122937>
- 436 27. Liu, Y. (2006). A simple thermodynamic approach for derivation of a general Monod equation for
437 microbial growth. *Biochemical Engineering Journal*, *31*(1), 102–105.
438 <https://doi.org/10.1016/j.bej.2006.05.022>
- 439 28. Marques, R., Von Stosch, M., Portela, R. M. C., Torres, C. A. V., Antunes, S., Freitas, F., Reis, M. A.
440 M., & Oliveira, R. (2017). Hybrid modeling of microbial exopolysaccharide (EPS) production: The case

- 441 of *Enterobacter* A47. *Journal of Biotechnology*, 246, 61–70.
442 <https://doi.org/10.1016/j.jbiotec.2017.01.017>
- 443 29. Padmanaban, S., Balaji, N., Muthukumar, C., & Tamilarasan, K. (2015). Statistical optimization of
444 process parameters for exopolysaccharide production by *Aureobasidium pullulans* using sweet potato
445 based medium. *3 Biotech*, 5(6), 1067–1073. <https://doi.org/10.1007/s13205-015-0308-3>
- 446 30. Plattes, M., & Lahore, H. M. F. (2023). Perspectives on the Monod model in biological wastewater
447 treatment. *Journal of Chemical Technology & Biotechnology*, 98(4), 833–837.
448 <https://doi.org/10.1002/jctb.7291>
- 449 31. Rangaswamy, B., Ramankutty Nair, R., Achuthan, C., & Isaac Sarojini, B. S. (2020). Computational
450 analysis of successional changes in the microbial population and community diversity of the immobilized
451 marine nitrifying bacterial consortium in a nitrifying packed bed bioreactor. *3 Biotech*, 10(12), 524.
452 <https://doi.org/10.1007/s13205-020-02510-z>
- 453 32. Ratib, N. R., Sabio, E. Y., Mendoza, C., Barnett, M. J., Clover, S. B., Ortega, J. A., Dela Cruz, F. M.,
454 Balderas, D., White, H., Long, S. R., & Chen, E. J. (2018). Genome-wide identification of genes directly
455 regulated by ChvI and a consensus sequence for ChvI binding in *Sinorhizobium meliloti*. *Molecular*
456 *Microbiology*, 110(4), 596–615. <https://doi.org/10.1111/mmi.14119>
- 457 33. Reuber, T. L., & Walker, G. C. (1993). Biosynthesis of succinoglycan, a symbiotically important
458 exopolysaccharide of *Rhizobium meliloti*. *Cell*, 74(2), 269–280. [https://doi.org/10.1016/0092-](https://doi.org/10.1016/0092-8674(93)90418-P)
459 [8674\(93\)90418-P](https://doi.org/10.1016/0092-8674(93)90418-P)
- 460 34. Ruiz, J., Arbib, Z., Álvarez-Díaz, P. D., Garrido-Pérez, C., Barragán, J., & Perales, J. A. (2013).
461 Photobiotreatment model (PhBT): A kinetic model for microalgae biomass growth and nutrient removal
462 in wastewater. *Environmental Technology*, 34(8), 979–991.
463 <https://doi.org/10.1080/09593330.2012.724451>
- 464 35. Sadiq, U. A. F. M., Yow, M. E., & Jamaian, S. S. (2018). The Extended Monod Model for Microalgae
465 Growth and Nutrient Uptake in Different Wastewaters. *International Journal of Engineering &*
466 *Technology*, 7(4.30), 200–204. <https://doi.org/10.14419/ijet.v7i4.30.22120>
- 467 36. Sellami, M., Frikha, F., Aribi, A., Taktak, I., Miled, N., & Rebah, F. B. (2018). Optimization of
468 wastewater based media for biopolymers production by *rhizobium leguminosarum*. *Environmental*
469 *Engineering and Management Journal*, 17(6), 1329–1335. Scopus.
470 <https://doi.org/10.30638/eemj.2018.132>

- 471 37. Sellami, M., Oszako, T., Miled, N., & Ben Rebah, F. (2015). Industrial wastewater as raw material for
472 exopolysaccharide production by *Rhizobium leguminosarum*. *Brazilian Journal of Microbiology*, 46(2),
473 407–413. <https://doi.org/10.1590/S1517-838246220140153>
- 474 38. Sellami, M., Oszako, T., Miled, N., & Rebah, F. B. (2015). Industrial wastewater as raw material for
475 exopolysaccharide production by *Rhizobium leguminosarum*. *Brazilian Journal of Microbiology*, 46(2),
476 407–413. Scopus. <https://doi.org/10.1590/S1517-838246220140153>
- 477 39. Sheng, G.-P., Yu, H.-Q., & Li, X.-Y. (2010). Extracellular polymeric substances (EPS) of microbial
478 aggregates in biological wastewater treatment systems: A review. *Biotechnology Advances*, 28(6), 882–
479 894. <https://doi.org/10.1016/j.biotechadv.2010.08.001>
- 480 40. Smith, L. H., Kitanidis, P. K., & McCarty, P. L. (1997). Numerical modeling and uncertainties in rate
481 coefficients for methane utilization and TCE cometabolism by a methane-oxidizing mixed culture.
482 *Biotechnology and Bioengineering*, 53(3), 320–331. [https://doi.org/10.1002/\(SICI\)1097-
483 0290\(19970205\)53:3<320::AID-BIT11>3.0.CO;2-O](https://doi.org/10.1002/(SICI)1097-0290(19970205)53:3<320::AID-BIT11>3.0.CO;2-O)
- 484 41. Solórzano, L. (1969). DETERMINATION OF AMMONIA IN NATURAL WATERS BY THE
485 PHENOLHYPOCHLORITE METHOD 1 1 This research was fully supported by U.S. Atomic Energy
486 Commission Contract No. ATS (11-1) GEN 10, P.A. 20. *Limnology and Oceanography*, 14(5), 799–801.
487 <https://doi.org/10.4319/lo.1969.14.5.0799>
- 488 42. Song, W., Lee, L. Y., You, H., Shi, X., & Ng, H. Y. (2020). Microbial community succession and its
489 correlation with reactor performance in a sponge membrane bioreactor coupled with fiber-bundle anoxic
490 bio-filter for treating saline mariculture wastewater. *Bioresource Technology*, 295, 122284.
491 <https://doi.org/10.1016/j.biortech.2019.122284>
- 492 43. Vajda, A. M., Barber, L. B., Gray, J. L., Lopez, E. M., Bolden, A. M., Schoenfuss, H. L., & Norris, D.
493 O. (2011). Demasculinization of male fish by wastewater treatment plant effluent. *Aquatic Toxicology*,
494 103(3–4), 213–221. <https://doi.org/10.1016/j.aquatox.2011.02.007>
- 495 44. Wang, K., Wang, Z., Ding, Y., Yu, Y., Wang, Y., Geng, Y., Li, Y., & Wen, X. (2023). Optimization of
496 Heterotrophic Culture Conditions for the Algae *Graesiella emersonii* WBG-1 to Produce Proteins. *Plants*,
497 12(12), Article 12. <https://doi.org/10.3390/plants12122255>
- 498 45. Xia, S., Song, Z., Jeyakumar, P., Shaheen, S. M., Rinklebe, J., Ok, Y. S., Bolan, N., & Wang, H. (2019).
499 A critical review on bioremediation technologies for Cr(VI)-contaminated soils and wastewater. *Critical*

- 500 *Reviews in Environmental Science and Technology*, 49(12), 1027–1078.
501 <https://doi.org/10.1080/10643389.2018.1564526>
- 502 46. Xiong, Z., Chen, H., Song, X., Xia, Y., & Ai, L. (2022). Rapid isolation of exopolysaccharide-producing
503 *Streptococcus thermophilus* based on molecular marker screening. *Journal of the Science of Food and*
504 *Agriculture*, 102(2), 862–867. <https://doi.org/10.1002/jsfa.11398>
- 505 47. Yadav, S., Tripathi, S., Purchase, D., & Chandra, R. (2023). Development of a biofilm-forming bacterial
506 consortium and quorum sensing molecules for the degradation of lignin-containing organic pollutants.
507 *Environmental Research*, 226, 115618. <https://doi.org/10.1016/j.envres.2023.115618>
- 508 48. Yan, Y., Zhou, J., Du, C., Yang, Q., Huang, J., Wang, Z., Xu, J., & Zhang, M. (2024). Relationship
509 between Nitrogen Dynamics and Key Microbial Nitrogen-Cycling Genes in an Intensive Freshwater
510 Aquaculture Pond. *Microorganisms*, 12(2), 266. <https://doi.org/10.3390/microorganisms12020266>
- 511 49. Yin, R., Cheng, J., Wang, J., Li, P., & Lin, J. (2022). Treatment of *Pseudomonas aeruginosa* infectious
512 biofilms: Challenges and strategies. *Frontiers in Microbiology*, 13, 955286.
513 <https://doi.org/10.3389/fmicb.2022.955286>
- 514 50. Youssef, H. H., Hamza, M. A., Fayez, M., Mourad, E. F., Saleh, M. Y., Sarhan, M. S., Suker, R. M.,
515 Eltahlawy, A. A., Nemr, R. A., El-Tahan, M., Ruppel, S., & Hegazi, N. A. (2016). Plant-based culture
516 media: Efficiently support culturing rhizobacteria and correctly mirror their in-situ diversity. *Journal of*
517 *Advanced Research*, 7(2), 305–316. <https://doi.org/10.1016/j.jare.2015.07.005>
- 518 51. Yuan, D., Wang, Y., & Qian, X. (2017). Variations of internal structure and moisture distribution in
519 activated sludge with stratified extracellular polymeric substances extraction. *International*
520 *Biodeterioration & Biodegradation*, 116, 1–9. <https://doi.org/10.1016/j.ibiod.2016.09.012>
- 521 52. Zhang, R., Zhou, Z., Ma, Y., Du, K., Sun, M., Zhang, H., Tu, H., Jiang, X., Lu, J., Tu, L., Niu, Y., &
522 Chen, P. (2023). Production of the exopolysaccharide from *Lactiplantibacillus plantarum* YT013 under
523 different growth conditions: Optimum parameters and mathematical analysis. *International Journal of*
524 *Food Properties*, 26(1), 1941–1952. <https://doi.org/10.1080/10942912.2023.2239518>
- 525 53. Zhao, J., Liu, S., Liu, N., Zhang, H., Zhou, Q., & Ge, F. (2019). Accelerated productions and
526 physicochemical characterizations of different extracellular polymeric substances from *Chlorella*
527 *vulgaris* with nano-ZnO. *Science of The Total Environment*, 658, 582–589.
528 <https://doi.org/10.1016/j.scitotenv.2018.12.019>

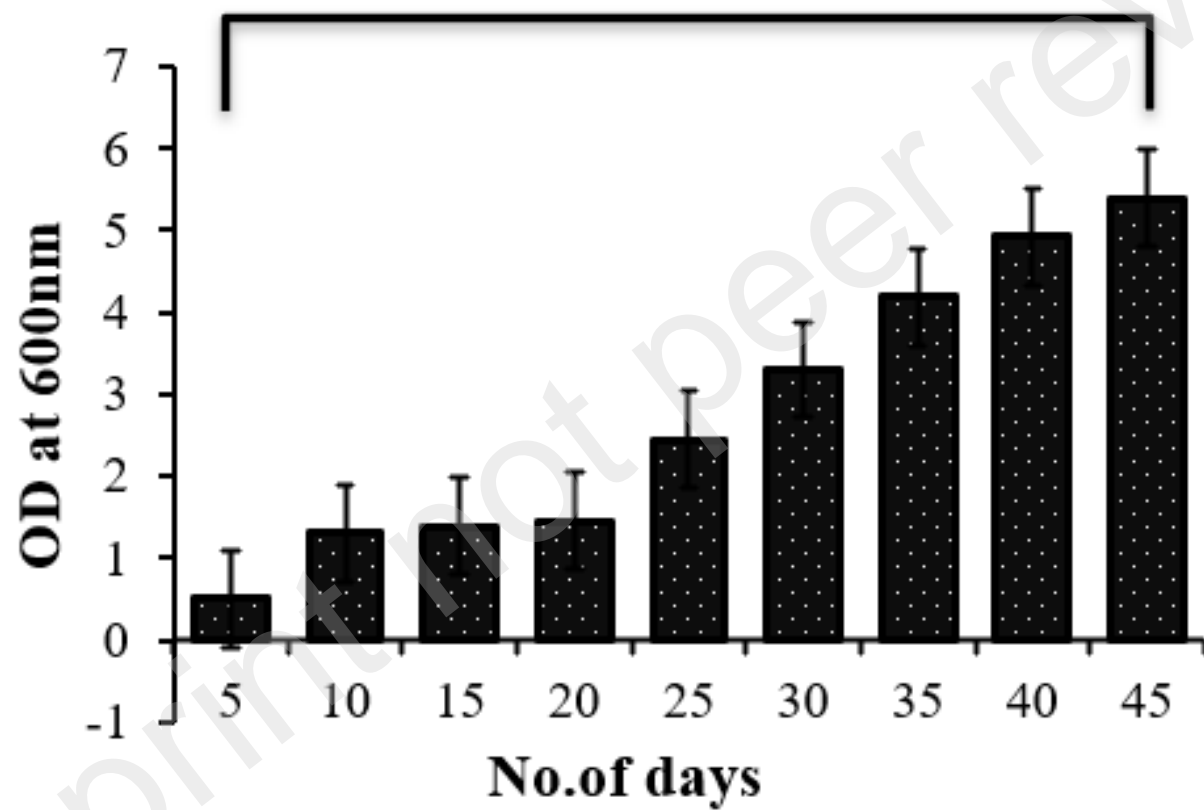
529 54. Zhou, Y., Chang, J., Zhang, M., Li, X., Luo, X., Li, W., Tian, Z., Zhang, N., Ni, B., Zhang, Y., & Lu, R.
530 (2025). GefB, a GGDEF domain-containing protein, affects motility and biofilm formation of *Vibrio*
531 *parahaemolyticus* and is regulated by quorum sensing regulators. *Gene*, 933, 148968.
532 <https://doi.org/10.1016/j.gene.2024.148968>
533

Table 1

Parameters derived for the kinetics of consortia growth and substrate utilisation

Parameters	Values obtained
μ_{max}	5.390
k_N	2.690
S_N	10
X_0	0.42
X_m	1.630

Consortia growth





2 μm



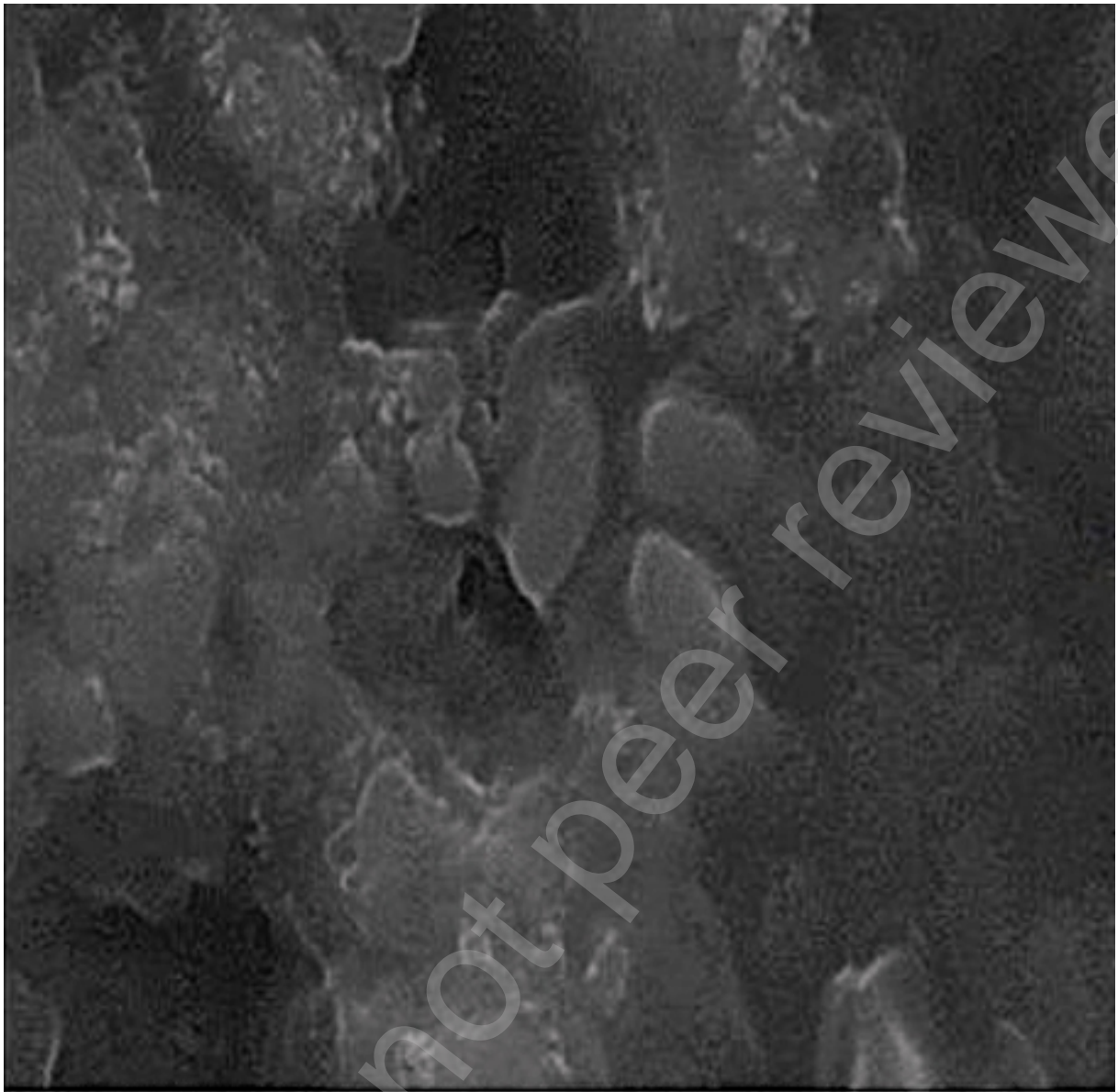
EHT = 20.00 kV

WD = 10.5 mm

Signal A = SE1

Mag = 10.00 K X





1 μ m

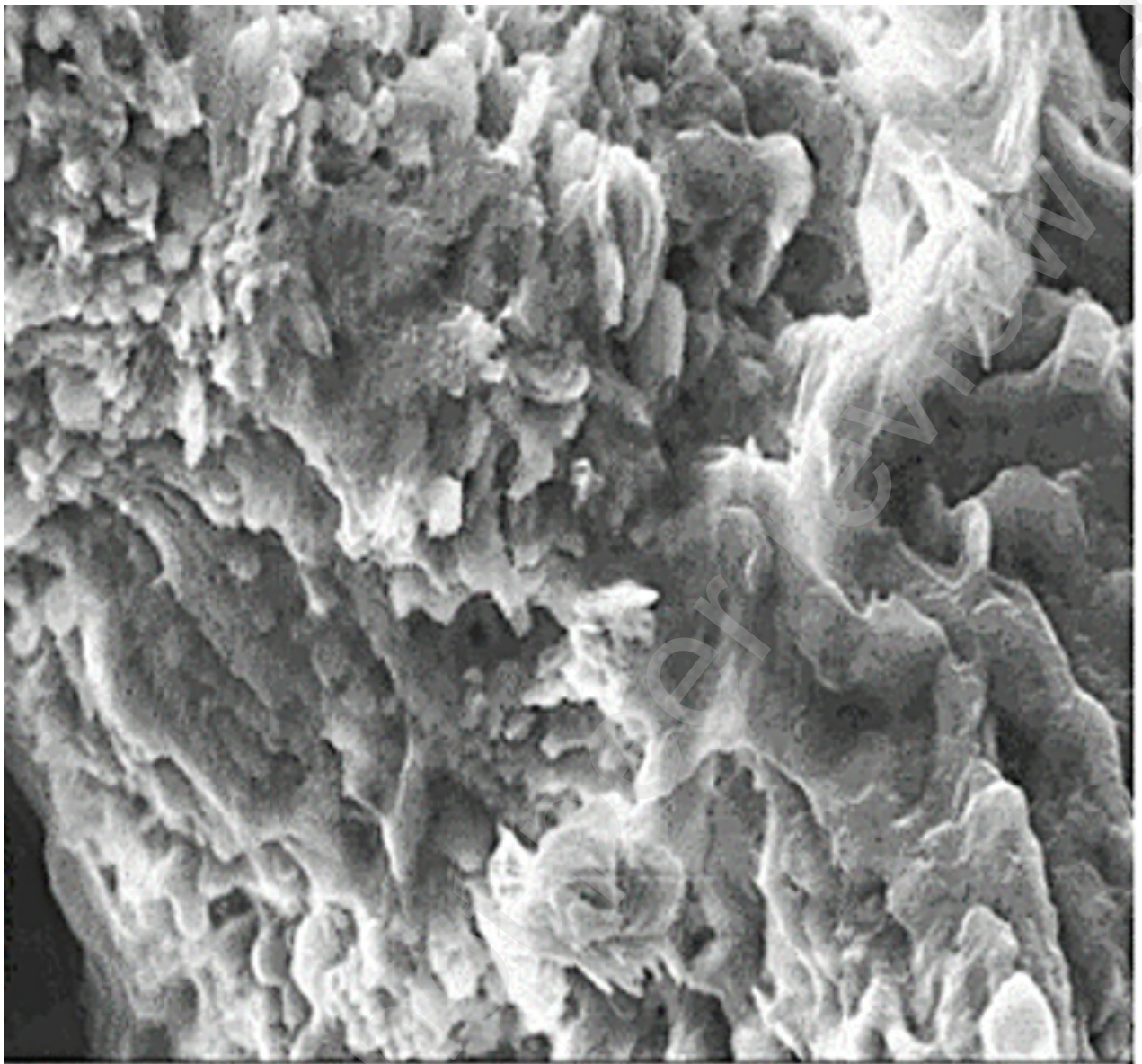
EHT = 20.00 kV

WD = 10.5 mm

Signal A = SE1

Mag = 2500 K X



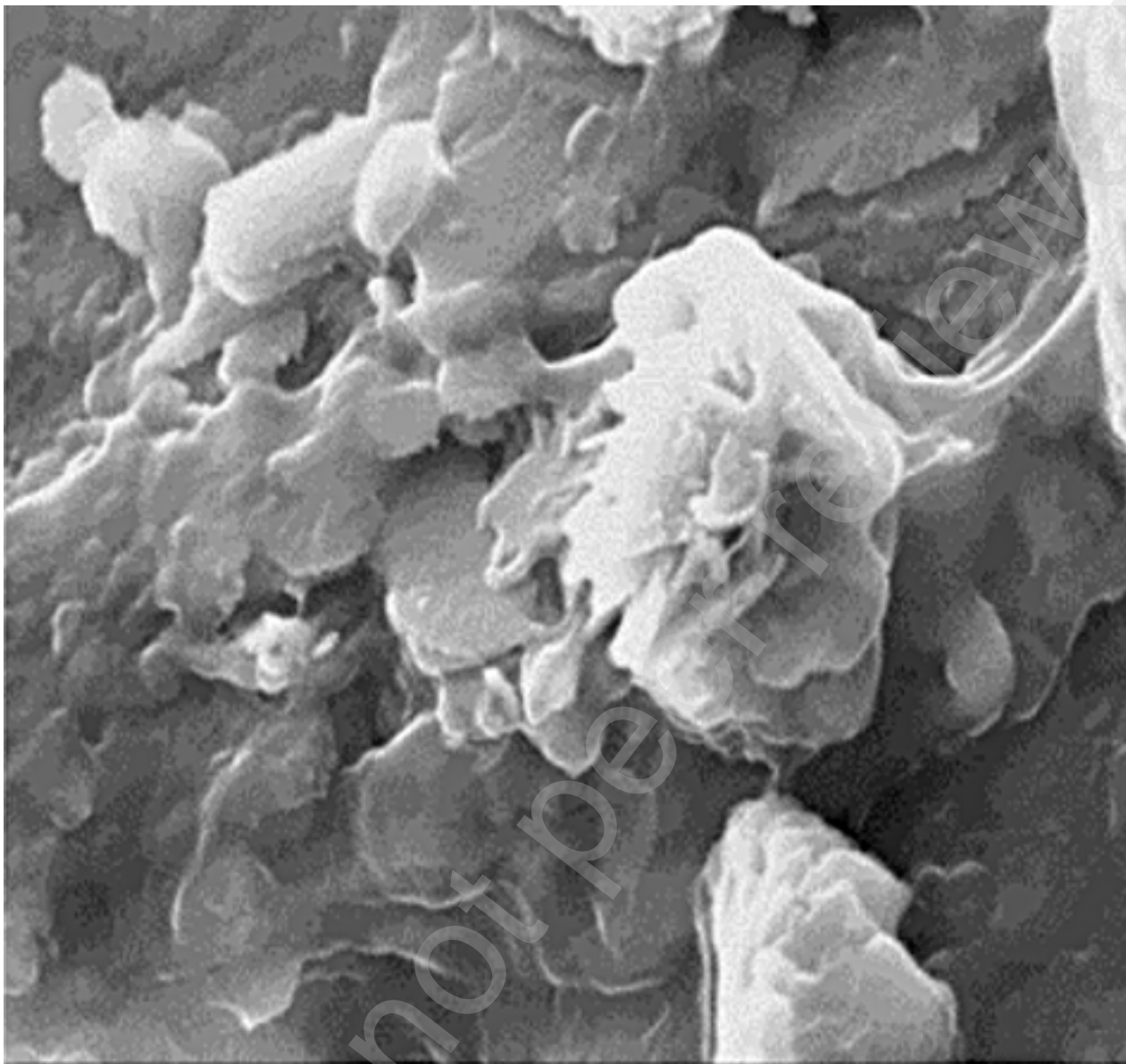


2 μ m
H

EHT = 15.00 kV
WD = 10.5 mm

Signal A = SE1
Mag = 5.00 K X





1 μ m
EHT = 15.00 kV
WD = 10.5 mm
Signal A = SE1
Mag = 20.00 K X
ZEISS

